

Interface contributions to spin relaxation in a short-period InAs/GaSb superlattice

J. T. Olesberg, Wayne H. Lau, Michael E. Flatté, C. Yu, E. Altunkaya, E. M. Shaw, T. C. Hasenberg, and Thomas F. Boggess
Optical Science and Technology Center and Department of Physics and Astronomy, The University of Iowa, Iowa City, Iowa 52242

(Received 14 June 2001; published 15 October 2001)

We describe measurements and analysis of the electronic spin relaxation in a short-period InAs/GaSb superlattice. Intrinsic inversion symmetry breaking due to tetrahedral bonding at the superlattice interfaces leads to spin relaxation over an order of magnitude greater than that expected from a continuum model. We extract the inversion asymmetry of the bonding character at the two distinct interfaces in this superlattice and describe how these (and future) measurements can be used to constrain fundamental interface parameters of superlattice envelope-function models.

DOI: 10.1103/PhysRevB.64.201301

PACS number(s): 72.25.Rb, 72.25.Fe

Spin relaxation near room temperature in III-V heterostructures is dominated by a precessional mechanism originating from an effective internal (crystal) magnetic field.¹⁻³ The rate of this spin relaxation depends on the magnitude of this internal field, which is in turn dependent on the spin-orbit coupling and the inversion asymmetry of the semiconductor structure. In a general nanostructure, the inversion asymmetry originates from three principal sources: the constituent bulk semiconductors in the nanostructure (bulk inversion asymmetry, or BIA), the global configuration of materials in the nanostructure (structural inversion asymmetry, or SIA), and bonding at the interfaces between bulk constituents that share no common atoms (native interface asymmetry, or NIA). The interface bonding contribution is of particular interest to those developing electronic structure models of superlattices, for NIA is a sensitive indicator of interface-specific changes in the electronic structure. Thus systems in which NIA dominates provide a unique window into the local electronic structure of nanostructure interfaces.

The extent to which NIA dominates is still unknown for most heterostructures. In symmetric GaAs/Al_xGa_{1-x}As quantum wells both SIA and NIA are negligible, and calculations based on BIA are very accurate.⁴ In single-interface modulation-doped heterostructures, however, SIA and BIA contribute comparably to the ground-state spin splitting.⁵ The possibility of NIA in In_xGa_{1-x}As/InP quantum wells, its dependence on interface contributions to envelope-function models, and its contribution to spin relaxation was pointed out in Ref. 6. Later calculations,⁴ however, indicated that BIA dominates in the thick wells which have been measured to date.³ To the authors' knowledge, the present structure is the first system in which NIA has been experimentally determined to provide the dominant contribution to the spin relaxation.

The structure we consider is a thin-layer superlattice of InAs and GaSb. We find extremely rapid spin relaxation in this system, over an order of magnitude faster than that predicted from the BIA contribution. The nominal repeating unit of 7 ML of InAs and 12 ML of GaSb has been characterized in detail by high-resolution X ray. We find SIA coming from compositional gradients measured in similar superlattices by cross-sectional scanning tunneling microscopy⁷ does not contribute significantly to the spin relaxation. With the addition of a single quantity parametrizing the NIA contribution

to the internal magnetic field the measured spin relaxation can be well-fit over most of the data's range of temperature and excitation energy. Thus, in this system the NIA contribution dominates. We conclude by describing the implications for generalized superlattice envelope-function models from these measurements of spin relaxation.

The superlattice, which was grown by molecular-beam epitaxy in an EPI 930 machine on an undoped GaSb substrate, is comprised of nine 7 ML thick InAs layers interleaved with eight 12 ML thick GaSb layers. To provide adequate thickness for optical measurements, ten repeats of this structure were grown with 200 Å thick AlSb strain-balancing barrier regions between them. This approach ensured coherent strain throughout the structure. Five-second antimony soaks were used after the growth of the InAs and GaSb layers in an attempt to control the interfaces. X-ray diffraction measurements taken in the ⟨211⟩ direction confirm that the quantum-well growth is coherently strained with the substrate. The sample, which is not intentionally doped, is *p* type with an estimated background impurity concentration (from Hall measurements on related samples) of 10¹⁶ cm⁻³. The structure has a room-temperature band gap of 4.07 μm determined from continuous-wave photoluminescence. The splitting between the band-edge heavy- and light-hole states is calculated to be 95 meV, indicating that circularly polarized light will generate close to 100% spin-polarized distributions in the conduction band.

Degenerate pump-probe measurements were performed using the idler output of a mid-infrared optical parametric oscillator (OPO) that has been described previously.⁸ The OPO, which is synchronously pumped by a mode-locked Ti:sapphire laser operating at 76 MHz, produces 10-20 mW of tunable mid-infrared output in ~120 fs (full width at half maximum) pulses with a typical bandwidth of 18 meV. The output from the OPO is split into two: an intense beam used to excite a nonequilibrium carrier population in the sample (40 μm spot size) and a weaker beam used to probe the change in transmission induced by the photogenerated carriers (30 μm spot size). The excitation density is estimated to be 2-5 × 10¹⁶ cm⁻³. The normalized change in transmission of the probe was measured as a function of delay, lattice temperature, excess optical energy, and optical polarization states of the two beams. Because the sample band-gap changes with temperature, the wavelength of the degenerate pump and probe were adjusted along with the sample tem-

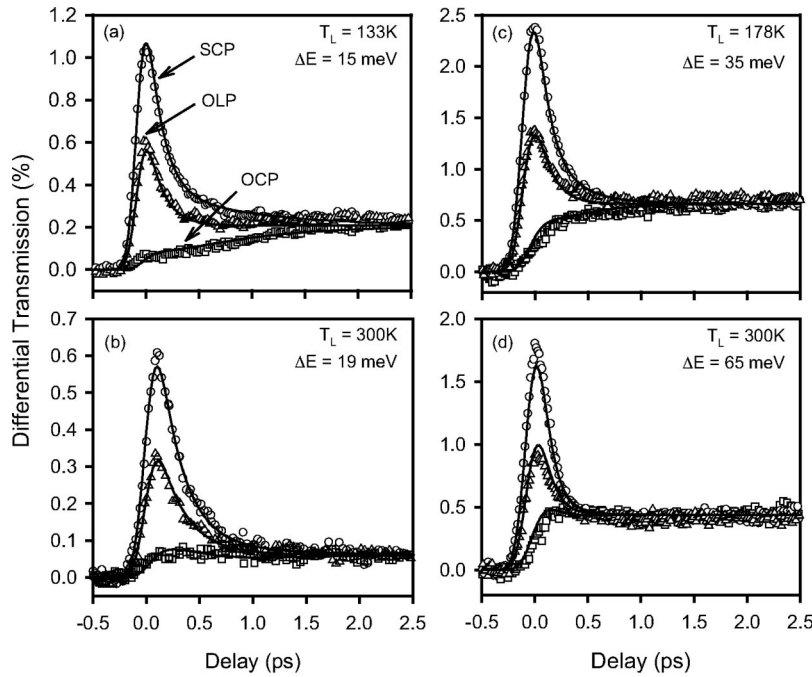


FIG. 1. Examples of spin dependent differential transmission for various lattice temperatures and excess excitation energies. The solid lines represent fits to the data using the model described in the text.

perature. To differentiate between effects due to the sample temperature and those due to excess optical energy, measurements were performed as a function of temperature for a fixed excess energy and as a function of excess energy for a fixed lattice temperature.

To evaluate the spin dynamics, measurements were conducted with the pump and probe of the same-linear (SLP), opposite-linear (OLP), same-circular (SCP), or opposite-circular (OCP) polarizations. The linear polarization configurations are insensitive to carrier spin, provide a measure of the total carrier population, and quantify the carrier scattering rates. They also allow us to identify coherent artifacts near zero delay and provide a useful comparison to the spin-sensitive measurements based on excitation and probing with circularly polarized pulses.

Representative measurements of polarization-dependent differential transmission are shown in Fig. 1 for various lattice temperatures and excess optical energies. In each case, the initial differential transmission signal depends strongly on the polarization state of the optical pump and probe, although all of the signals converge within 2 ps for temperatures between 80 K and 300 K. The OLP data indicate that the optically generated carriers completely thermalize in less than 0.5 ps, although the time to equilibrate with the lattice may be longer. For this structure, the OLP and SLP curves (not shown) are identical within experimental error, indicating no measurable coherent artifact. This result is also supported by the fact that the average of the SCP and OCP curves is, again within experimental error, identical to the OLP curve. The SCP and OCP data are indicative of relaxation of an initially fully spin-polarized distribution into a randomly polarized distribution on a time scale of a picosecond or less.

Quantitative analysis of the spin relaxation from differential transmission experiments is typically accomplished by assuming thermalization times T_{th} and equilibration times

T_{equil} much more rapid than the spin relaxation time T_1 . This permits elimination of the spin-independent signal by fitting the difference in the SCP and OCP data to a decaying exponential.⁹ In the present situation, however, an unusual regime exists where T_1 is sometimes comparable to T_{th} , and T_{equil} is usually greater than T_1 . In this regime we extract T_1 using a general linear interaction analysis. Specifically, we model the data using the convolution of a response function with the autocorrelation of the optical pulses. The short-time response function is taken to consist of the product of a fast spin-independent exponential decay (characterized by T_{th}) and a spin-dependent signal that either decays (SCP) or rises (OCP) exponentially to a constant value. Least-squares fits of the data to this model are shown by the solid curves in Fig. 1. The model provides a very satisfactory fit for the SCP, OCP, and OLP configurations for each data set, and we estimate the error in the extracted T_1 and T_{th} to be $<5\%$. We extract spin relaxation times of 850, 682, 328, and 163 fs for the measurement results shown in Figs. 1(a)–1(d). These short T_1 times are comparable to those reported for GaSb/AlSb ($T_1 = 517$ fs) and $\text{Ga}_x\text{As}_{1-x}\text{Sb}/\text{AlSb}$ ($T_1 = 420$ fs) quantum wells at room temperature.¹⁰ Note spin-flip times were reported in Ref 10; spin-flip times are twice T_1 .

The dependence of the spin relaxation time on lattice temperature and excess optical energy is summarized in Table I. We saw no significant changes in T_{th} and T_1 upon reducing the pump power. The data indicate that, for a given excess optical energy, the spin relaxation time exhibits *little, if any*, temperature dependence from 80 K to 300 K. This is illustrated in Fig. 2(a), which shows the spin relaxation time as a function of lattice temperature for excess optical energies of 15, 25, and 35 meV. The lack of dependence on lattice temperature would appear to be inconsistent with spin relaxation through precessional decoherence of an electron gas in thermal equilibrium with the lattice, hence $T_1 \ll T_{equil}$. Figure

TABLE I. Measured spin relaxation time (T_1) and carrier thermalization time (T_{th}) as a function of lattice temperature (T_L) and optical excess energy (ΔE). The wavelength of the degenerate pump and probe pulses is λ . Errors in T_1 and T_{th} are $<5\%$.

ΔE (meV)	T_L (K)	λ (μm)	T_1 (fs)	T_{th} (fs)
13	300	3.90	972	213
15	260	3.77	808	225
	220	3.65	944	142
	178	3.55	1078	130
	133	3.45	850	145
	80	3.36	1069	74
19	300	3.83	682	247
	178	3.36	328	138
25	300	3.77	389	289
	178	3.45	473	174
35	300	3.65	338	285
	178	3.36	328	138
45	300	3.55	262	193
	178	3.45	473	174
55	300	3.45	183	140
	178	3.45	473	174
65	300	3.36	163	107
	178	3.45	473	174

2(b) shows, however, that the measured T_1 decreases significantly with increasing excess optical energy, reaching a time scale comparable to the optical pulse autocorrelation at excess energies of ~ 60 meV. Such behavior is consistent with the strong energy dependence of the conduction-band spin splitting.¹¹

To model the spin relaxation rate we assume $T_{th} < T_1 < T_{equil}$, and therefore the optically excited carriers

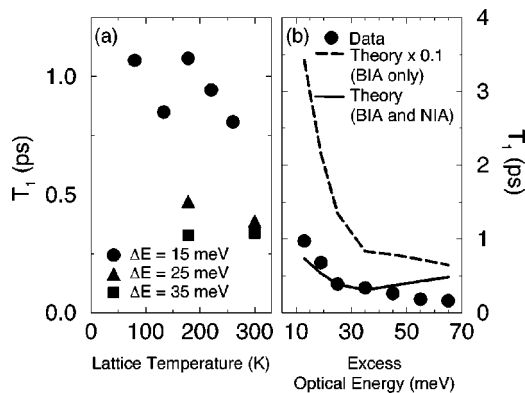


FIG. 2. (a) Dependence of spin lifetime, T_1 , on lattice temperature for excess optical energies of 15, 25, and 35 meV. The value for 300 K and an excess energy of 15 meV is the linear interpolation of the values for excess energies of 13 and 19 meV. (b) Dependence of T_1 on the excess optical energy of the pump and probe pulses for a lattice temperature of 300 K. Also shown are theory without interface contributions (dashed line) and with an antisymmetric interface contribution of 500 meV (solid line).

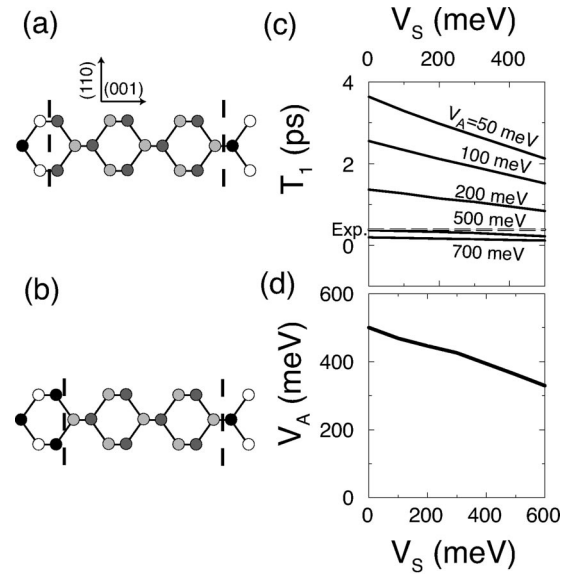


FIG. 3. (a) Asymmetric bonding character at the two interfaces. The shades indicate, in order of darkness, As, Sb, Ga, and In. Dashed lines indicate the location of the interface bonds. (b) asymmetric bonding orientation of In-Sb bonds at the two interfaces. (c) Calculated T_1 as a function of antisymmetric (V_A) and symmetric (V_S) HH-LH coupling at an excess energy of 25 meV. (d) Pairs of V_A and V_S which fit the experimental data.

scatter quasielastically in a narrow energy range of states given by the optical pulse's spectrum. The relevant crystal magnetic fields correspond to the crystal fields at those energies. Contributions from BIA are calculated as described previously.⁴ The results including BIA are shown on Fig. 2(b), and differ from the measurements by a factor of 36. Including SIA from typical compositional gradients⁷ changes the results by $\sim 20\%$. The remaining discrepancy must come from NIA. The origin of NIA is evident in Fig. 3. Different bonding types at the two interfaces [Fig. 3(a)] generate inversion asymmetry, but even if the bonding types at both the InAs-on-GaSb and the GaSb-on-InAs interfaces are the same [e.g., InSb in Fig. 3(b)], the bonds at the two interfaces are rotated by 90° around (001), and thus inversion asymmetric. Within an envelope-function formalism for superlattice electronic structure the presence of these interface bonds can be considered as an effective off-diagonal valence-band coupling, directly mixing the heavy and light holes over a half-monolayer thickness at the interface.⁶ Just as an ordinary valence-band offset can be viewed within an empirical model as a quantity determined from experiment, the off-diagonal valence-band coupling can be determined from the above spin relaxation time measurements. Using an antisymmetric coupling of 500 meV, InSb bonds at one interface and GaAs bonds at the other, we find good agreement with experiment [shown in Fig. 2(b)]. The small deviations at higher energies may be associated with carrier cooling ($T_{equil} \sim T_1$), or with probing the tail of a thermalized distribution. The value of 500 meV is comparable to that estimated for $\text{In}_x\text{Ga}_{1-x}\text{As}/\text{InP}$ quantum wells.⁶

If the interface bonding type were pure, say InSb-like, then the parameter appropriate for InSb interfaces would be

determined. The interfaces here, however, are likely both mixed—therefore an unknown linear combination of the GaAs and InSb parameters is measured. Further measurements of spin relaxation in short-period superlattices, combined with direct characterization of the interface bonding,¹² will permit the disentangling of the contribution from GaAs-like and InSb-like bonds. For this structure, however, symmetric changes (same at both interfaces) to the HH-LH coupling up to 600 meV only slightly reduce the required antisymmetric coupling to fit the data. Shown in Fig. 3(c) are calculated T_1 's for antisymmetric and symmetric couplings for excess energy 25 meV at 300 K. Figure 3(d) shows the pairs of V_A and V_S which fit the data. As mentioned above, compositional gradients characteristic of high-quality growth of these structures, as well as whether the band edges at the interfaces are chosen to be those of InSb or GaAs bonds have a $\sim 20\%$ effect on calculated T_1 's, resulting in a $\sim 10\%$ effect on the values of the HH-LH coupling extracted from the theory-experiment comparison. We estimate a total uncertainty in the V_A , V_S pairs of 100 meV from these effects as

well as experimental uncertainties in layer thickness and T_1 's.

Here a series of coordinated experiments and calculations have been applied to a short-period InAs/GaSb superlattice to determine the value of the HH-LH coupling at the interfaces due to tetrahedral bonding coordination. For this system the spin relaxation is dominated by contributions from the interface. The extracted value of 500 ± 100 meV for the asymmetric component (in the absence of a symmetric component) is comparable to that estimated for $\text{In}_x\text{Ga}_{1-x}\text{As}/\text{InP}$ quantum wells. Studies along these lines can tightly constrain atomistic calculations considering the influence of interface structure on nanostructure electronic properties.

We would like to acknowledge conversations with D.D. Awschalom. This work was supported in part by DARPA Contract Nos. MDA972-01-C-0002, DARPA/ARO DAAD19-01-1-0490, NSF ECS-9707799, and ECS-0000556.

-
- ¹M.I. D'yakonov and V.I. Perel', Zh. Éksp. Teor. Fiz. **60**, 1954 (1971) [Sov. Phys. JETP **33**, 1053 (1971)].
- ²A. Tackeuchi, S. Muto, T. Inata, and T. Fujii, Appl. Phys. Lett. **56**, 2213 (1990); A. Tackeuchi, Y. Nishikawa, and O. Wada, *ibid.* **68**, 797 (1996); R. Terauchi *et al.*, Jpn. J. Appl. Phys., Part 1 **38**, 2549 (1999).
- ³A. Tackeuchi, O. Wada, and Y. Nishikawa, Appl. Phys. Lett. **70**, 1131 (1997); J.T. Hyland, G.T. Kennedy, A. Miller, and C.C. Button, Semicond. Sci. Technol. **14**, 215 (1999).
- ⁴W.H. Lau, J.T. Olesberg, and M.E. Flatté, Phys. Rev. B **64**, 161301 (2001).
- ⁵P. Pfeffer and W. Zawadzki, Phys. Rev. B **52**, R14 332 (1995); P. Pfeffer, *ibid.* **55**, R7359 (1997); P. Pfeffer and W. Zawadzki, *ibid.* **59**, R5312 (1999).
- ⁶O. Krebs and P. Voisin, Phys. Rev. Lett. **77**, 1829 (1996); L. Vervoort, R. Ferreira, and P. Voisin, Semicond. Sci. Technol. **14**, 227 (1999).
- ⁷J. Steinshnider, J. Harper, M. Weimer, C.-H. Lin, S.S. Pei, and D.H. Chow, Phys. Rev. Lett. **85**, 4562 (2000).
- ⁸S.W. McCahon, S.A. Anson, D.-J. Jang, and T.F. Boggess, Opt. Lett. **20**, 2309 (1995).
- ⁹See, e.g., S. Bar-Ad and I. Bar-Joseph, Phys. Rev. Lett. **68**, 349 (1992).
- ¹⁰K.C. Hall, S.W. Leonard, H.M. van Driel, A.R. Kost, E. Selvig, and D.H. Chow, Appl. Phys. Lett. **75**, 4156 (1999).
- ¹¹E.L. Ivchenko and G.E. Pikus, *Superlattices and Other Heterostructures*, 2nd ed. (Springer, New York, 1997).
- ¹²J. Steinshnider, M. Weimer, R. Kaspi, and G.W. Turner, Phys. Rev. Lett. **85**, 2953 (2000).